

## Instability of current sheets and formation of plasmoid chains

N. F. Loureiro

*Center for Multiscale Plasma Dynamics, University of Maryland, College Park, Maryland 20742-3511, USA and Plasma Physics Laboratory, Princeton University, Princeton, New Jersey 08543, USA*

A. A. Schekochihin

*Blackett Laboratory, Imperial College, London SW7 2BW, United Kingdom and King's College, University of Cambridge, Cambridge CB2 1ST, United Kingdom*

S. C. Cowley

*Blackett Laboratory, Imperial College, London SW7 2BW, United Kingdom and Department of Physics and Astronomy, UCLA, Los Angeles, California 90095-1547, USA*

(Received 21 June 2007; accepted 21 August 2007; published online 29 October 2007)

Current sheets formed in magnetic reconnection events are found to be unstable to high-wavenumber perturbations. The instability is very fast: its maximum growth rate scales as  $S^{1/4}v_A/L_{CS}$ , where  $L_{CS}$  is the length of the sheet,  $v_A$  the Alfvén speed, and  $S$  the Lundquist number. As a result, a chain of plasmoids (secondary islands) is formed, whose number scales as  $S^{3/8}$ .  
© 2007 American Institute of Physics. [DOI: 10.1063/1.2783986]

Magnetic reconnection is a plasma phenomenon in which oppositely directed magnetic field lines are driven together, break, and rejoin in a topologically different configuration. It is an essential element in our understanding of the solar flares and the magnetotail,<sup>1–3</sup> where it is directly observed,<sup>4,5</sup> as well as of other astrophysical plasmas. On Earth, it plays a crucial role in the dynamics of magnetically confined plasmas in fusion devices.<sup>6</sup>

There are two standard reconnection models: The Sweet-Parker (SP) model<sup>7,8</sup> and the Petschek model.<sup>9</sup> The latter is very appealing as it predicts fast reconnection rates similar to the observed ones. However, numerical simulations have consistently failed to reproduce it unless a spatially inhomogeneous anomalous resistivity is used<sup>10</sup> or Hall physics is invoked.<sup>3,11</sup> In contrast, the SP reconnection, characterized by long current sheets ( $\sim$  system size) and slow reconnection rates  $\propto \eta^{1/2}$ , where  $\eta$  is the plasma resistivity, is routinely observed both in experiments<sup>12</sup> and in simulations.

The break up of current sheets and formation of plasmoids (secondary islands) appears to be a generic feature of reconnecting systems. Plasmoids have been observed both in solar flares<sup>13</sup> and in the magnetotail.<sup>14</sup> In numerical simulations, plasmoid formation has been reported in many different setups, from fluid<sup>15,16</sup> to fully kinetic.<sup>17,18</sup> Plasmoids have been popular in theories of magnetic reconnection and related phenomena. For example, they have been invoked as a plausible mechanism for accelerating reconnection, either by decreasing the effective length of the SP current sheet and/or by triggering anomalous-resistivity mechanisms associated with small-scale plasma effects.<sup>19</sup> A multiple-plasmoid scenario has been suggested to explain the production of energetic electrons during reconnection events;<sup>20</sup> it has been conjectured that periodic ejection of plasmoids in star-disk systems could account for the knot-like structures observed in stellar jets.<sup>21</sup>

A theoretical understanding of the mechanism whereby the plasmoids are formed has, however, been lacking. It has

been believed that plasmoid formation is due to a standard tearing instability<sup>22</sup> of the current sheet. Bulanov *et al.*<sup>23</sup> considered the onset of such an instability by taking into account a linear outflow along the sheet and repeating the standard tearing-mode calculation. While this gave a qualitative indication of the mildly stabilizing role of the outflow, it was necessarily a nonrigorous approach because the resistivity could not be neglected anywhere inside the current sheet and no other small parameter was available. In this Letter, we pursue a different strategy by considering a large-aspect-ratio sheet and using the inverse of its aspect ratio as the small parameter. We show that multiple plasmoids form and that, unlike in Bulanov *et al.*,<sup>23</sup> the instability is very fast, with a rate much larger than the ideal (Alfvénic) rate.

Theoretical estimates for the speed of magnetic reconnection in natural systems are usually based on the idea that a current sheet is formed (Fig. 1), with the length  $L_{CS}$  determined by the system's global properties and the width  $L_{CS}/\sqrt{S}$ , where  $S=v_AL_{CS}/\eta$  is the Lundquist number,  $v_A$  is the upstream Alfvén speed, and  $\eta$  is the magnetic diffusivity. Let us consider such a current sheet, and ask if it can be stable over any significant period of time. The SP reconnection time is  $(L_{CS}/v_A)\sqrt{S}$ . If we consider times much shorter than this time, we can determine the structure of the current sheet by seeking a stationary solution of the induction equation

$$\partial_t \mathbf{B} + \mathbf{u} \cdot \nabla \mathbf{B} = \mathbf{B} \cdot \nabla \mathbf{u} - \mathbf{B} \nabla \cdot \mathbf{u} + \eta \nabla^2 \mathbf{B}, \quad (1)$$

where  $\mathbf{u}$  is the velocity field and  $\mathbf{B}$  the magnetic field, which we will measure in velocity units. While the desired resistive equilibrium is stationary, it is not static. It is a consistent feature of current sheets, both measured<sup>12</sup> and simulated,<sup>24</sup> that they support linear outflows along themselves. If incompressibility is assumed and the reconnection is considered in two dimensions  $(x, y)$  with a current sheet along the  $y$  axis, then, inside the current sheet,  $u_x = -\Gamma_0 x$  and  $u_y = \Gamma_0 y$ . Here,  $\Gamma_0 = 2v_A/L_{CS}$ , so the outflows are Alfvénic. Obviously, this

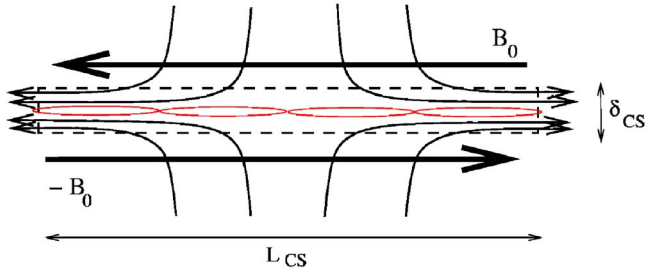


FIG. 1. (Color online) Schematic drawing of the current sheet with in- and outflows and a forming plasmoid chain.

choice of  $\mathbf{u}$  is a drastic simplification of the real flow profile (ignoring, for example, the flow vorticity). It is only intended as a minimal model incorporating what we believe to be the key feature, namely the linearly increasing Alfvénic outflow.

A simple equilibrium solution  $\mathbf{B}_0$  of Eq. (1) exists that accommodates this flow pattern:  $B_{0x}=0$ , and  $B_{0y}=B_{0y}(x)$  satisfies

$$\delta_{CS}^2 \partial_x^2 B_{0y} + \partial_x(x B_{0y}) = 0, \quad (2)$$

where  $\delta_{CS}=(\eta/\Gamma_0)^{1/2}$  is the characteristic width of the current sheet. The solution of this equation that vanishes and changes sign at  $x=0$  (the center of the sheet) is  $B_{0y}=v_A f(\xi)$ , where  $\xi=x/\delta_{CS}$  and

$$f(\xi) = \alpha e^{-\xi^2/2} \int_0^\xi dz e^{z^2/2}. \quad (3)$$

The integration constant  $\alpha$  is chosen by matching this solution with the magnetic field outside the sheet:  $B_{0y}=\pm v_A$ , which is a solution of Eq. (1) with constant inflows  $u_x = \mp u_0$ ,  $u_y=0$ . In order to complete our simple model of the current sheet, we must choose a suitable point  $x=\pm x_0$  at which the inside and outside solutions can be matched. The flow is discontinuous at this point:  $\mathbf{u}=(u_0, 0)$  for  $x < -x_0$ ,  $\mathbf{u}=(-\Gamma_0 x, \Gamma_0 y)$  for  $-x_0 < x < x_0$ , and  $\mathbf{u}=(-u_0, 0)$  for  $x > x_0$ , where  $u_0=\Gamma_0 x_0$ . We consider this to be an acceptable simplification of the real, more complicated, and continuous, flow profile. The natural matching point is the point where  $B_{0y}(x)$  has its maximum (minimum),  $B_{0y}(\pm x_0)=0$ , and where, therefore, the current vanishes. This gives  $x_0=\xi_0 \delta_{CS}$ , where  $\xi_0 \approx 1.31$ . We then require  $f(\pm \xi_0)=\pm 1$ , so  $\alpha=\xi_0$ . The equilibrium magnetic field and current are plotted in Fig. 2.

We shall show that this equilibrium is subject to a very fast linear instability. We consider the two-dimensional case and solve the reduced MHD equations.<sup>25</sup> Denoting  $\{\phi, \psi\} \equiv \partial_x \phi \partial_y \psi - \partial_y \phi \partial_x \psi$ , we have

$$\partial_t \nabla_\perp^2 \phi + \{\phi, \nabla_\perp^2 \phi\} = \{\psi, \nabla_\perp^2 \psi\}, \quad (4)$$

$$\partial_t \psi + \{\phi, \psi\} = \eta \nabla_\perp^2 \psi + E_0. \quad (5)$$

Here,  $\phi$  and  $\psi$  are the stream and flux functions, respectively, of the in-plane velocity and magnetic field, so  $\mathbf{u}=(-\partial_y \phi, \partial_x \phi)$ ,  $\mathbf{B}=(-\partial_y \psi, \partial_x \psi)$ . Equation (4) is the curl of the (inviscid) equation for an incompressible conducting fluid; Eq. (5) is the induction equation (1) uncoupled.  $E_0$  is the equilibrium electric field, which must satisfy  $\partial_x E_0=0$ . The model of equilibrium flows described above corresponds to  $\phi_0$

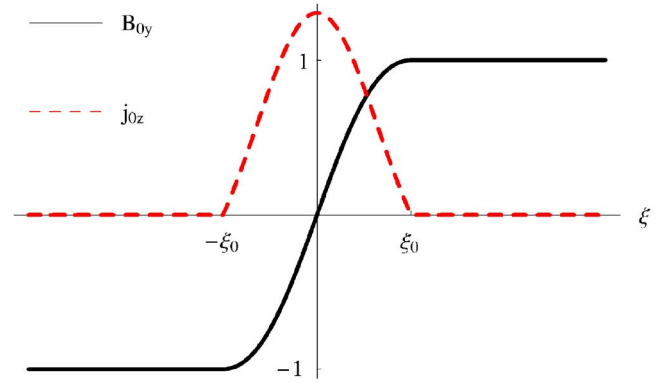


FIG. 2. (Color online) The equilibrium magnetic field  $B_{0y}$  and the current density  $j_{0z}=\partial_x B_{0y}$  (normalized to  $v_A$  and  $v_A/\delta_{CS}$ , respectively).

$=\Gamma_0 x y$  for  $|x| < x_0$  and  $\phi_0=\pm \Gamma_0 x_0 y$  for  $|x| > x_0$ , which satisfies Eq. (4). The magnetic-field profile (3) satisfies Eq. (5), provided we choose  $E_0=-v_A \Gamma_0 \delta_{CS} \alpha$  for  $|x| < x_0$  and  $E_0=-v_A \Gamma_0 x_0$  for  $|x| > x_0$ .

Let us consider small perturbations to this equilibrium, so  $\psi=\psi_0+\delta\psi$ ,  $\phi=\phi_0+\delta\phi$ , and linearize Eqs. (4) and (5). If we seek solutions in the form  $\delta\phi(x, y, t)=\phi_1(x, t) \times \exp[ik(t)y]$  and  $\delta\psi(x, y, t)=\psi_1(x, t) \exp[ik(t)y]$ , where  $k(t)=k_0 \exp(-\Gamma_0 t)$ , then  $\phi_1$  and  $\psi_1$  satisfy

$$\begin{aligned} (\partial_x^2 - k^2) \partial_t \phi_1 - \Gamma_0 x \partial_x (\partial_x^2 - k^2) \phi_1 + 2\Gamma_0 k^2 \phi_1 \\ = [B_{0y}(x)(\partial_x^2 - k^2) - B_{0y}''(x)] ik \psi_1, \end{aligned} \quad (6)$$

$$\partial_t \psi_1 - \Gamma_0 x \partial_x \psi_1 - B_{0y}(x) ik \phi_1 = \eta (\partial_x^2 - k^2) \psi_1. \quad (7)$$

We now seek exponentially growing solutions  $\phi_1(x, t)=-i\Phi(x) \exp(\gamma t)$  and  $\psi_1(x, t)=\Psi(x) \exp(\gamma t)$ . A solvable eigenvalue problem for  $\gamma$  can be obtained if we assume  $\gamma \gg \Gamma_0$ , so the terms proportional to  $\Gamma_0$  can be neglected and  $k(t) \approx k_0$ . Note that the presence of the linear in- and outflows in this approximation is only felt via the equilibrium profile  $B_{0y}(x)$ . Rewriting Eqs. (6) and (7) in terms of the dimensionless variable  $\xi=x/\delta_{CS}$  and denoting  $\kappa=k_0 v_A/\Gamma_0=k_0 L_{CS}/2$ ,  $\epsilon=(\eta \Gamma_0)^{1/2}/v_A=2\delta_{CS}/L_{CS}$ , and  $\lambda=\gamma/\Gamma_0 \kappa$ , we get

$$\lambda (\Phi'' - \kappa^2 \epsilon^2 \Phi) = -f(\xi) (\Psi'' - \kappa^2 \epsilon^2 \Psi) + f''(\xi) \Psi, \quad (8)$$

$$\lambda \Psi - f(\xi) \Phi = \frac{1}{\kappa} (\Psi'' - \kappa^2 \epsilon^2 \Psi), \quad (9)$$

where the derivatives are with respect to  $\xi$ .

The eigenvalue problem given by Eqs. (8) and (9) is mathematically similar to the standard tearing mode problem,<sup>22</sup> except that the role of resistivity is played by  $1/\kappa$ . We shall assume that this parameter is small; i.e., we shall look for high-wavenumber perturbations of the current sheet. Another small parameter is  $\epsilon=(2/S)^{1/2}$ , which is the inverse aspect ratio of the sheet. We shall assume that  $\kappa \epsilon \ll 1$ . All these assumptions will prove to be correct for the fastest growing modes.

We now proceed as in the standard tearing mode calculation, considering first the outer region ( $\xi \sim 1$ ) and then the inner region ( $\xi \ll 1$ ).

*Outer region.* The behavior here is “ideal.” Assuming

that  $(1/\kappa) \ll \lambda \ll 1$ , we get from Eq. (9) that  $\Phi = \lambda \Psi / f(\xi)$ , and then from Eq. (8),

$$\Psi'' = \left[ \frac{f''(\xi)}{f(\xi)} + \kappa^2 \epsilon^2 \right] \Psi. \quad (10)$$

Given the functional form of the equilibrium  $f(\xi)$ , solving this equation exactly is difficult. Instead, we shall solve it perturbatively, using  $\kappa^2 \epsilon^2 \ll 1$ . Neglecting  $\kappa^2 \epsilon^2$  to lowest order, we have an equation whose one solution is  $f(\xi)$ . It is then easy to find the second solution, so the general solution can be written as follows:

$$\Psi^\pm(\xi) = C_1^\pm f(\xi) + C_2^\pm f(\xi) \int_{\pm \xi_0}^{\xi} \frac{dz}{f^2(z)}, \quad (11)$$

where  $C_1^\pm$  and  $C_2^\pm$  are constants of integration and  $\pm$  refers to the solution at positive and negative values of  $\xi$ . We ask for the solution (but not its derivative) to be continuous at  $\xi=0$ . At small  $\xi$ , we have  $f(\xi) \approx \alpha \xi$ , so the integral in Eq. (11) is dominated by its upper limit and we find that  $C_2^+ = C_2^- = -\alpha \Psi(0)$ .

The constants  $C_1^\pm$  are found by matching the solution (11) to the outer solution at  $|\xi| > \xi_0$  (outside the current sheet). There we have, instead of Eq. (10),

$$\Psi'' = \kappa^2 \epsilon^2 \Psi, \quad (12)$$

so  $\kappa^2 \epsilon^2$  can no longer be neglected. The solution that decays at  $\xi \rightarrow \pm \infty$  is  $\Psi^\pm = C_3^\pm \exp(\mp \kappa \epsilon \xi)$ . Matching this solution and its derivative to the solution (11) and using  $f(\pm \xi_0) = \pm 1$  and  $f'(\pm \xi_0) = 0$ , we get  $C_2^\pm = \pm \alpha \Psi(0) / \kappa \epsilon$  and  $C_3^\pm = \alpha \Psi(0) \times \exp(\kappa \epsilon \xi_0) / \kappa \epsilon$ . Thus, for  $|\xi| < \xi_0$ ,

$$\Psi^\pm(\xi) = \pm \frac{\alpha \Psi(0)}{\kappa \epsilon} f(\xi) - \alpha \Psi(0) f(\xi) \int_{\pm \xi_0}^{\xi} \frac{dz}{f^2(z)}, \quad (13)$$

and for  $|\xi| > \xi_0$ ,

$$\Psi^\pm(\xi) = \frac{\alpha \Psi(0)}{\kappa \epsilon} \exp[\kappa \epsilon (\xi_0 \mp \xi)]. \quad (14)$$

This outer solution is plotted in Fig. 3. It has a discontinuous derivative at  $\xi=0$  and is a classic unstable eigenfunction known from the tearing-mode problem. The instability parameter  $\Delta' = [\Psi'(0+) - \Psi'(0-)] / \Psi(0)$  is

$$\Delta' = \frac{2\alpha^2}{\kappa \epsilon} + \alpha^2 \left[ \int_{-\xi_0}^{\xi_0} \frac{dz}{f^2(z)} \right], \quad (15)$$

where  $[\dots]$  denotes the nonsingular part of the integral. The second term in Eq. (15), which is equal to 0.57, can be dropped compared to the first, so to lowest order we have simply  $\Delta' = 2\alpha^2 / \kappa \epsilon$ .<sup>31</sup>

*Inner region.* Here,  $\xi \ll 1$  and we can assume  $f(\xi) \approx \alpha \xi$ . Equations (8) and (9), assuming  $\partial_\xi \gg 1$ , become

$$\lambda \Phi'' = -\alpha \xi \Psi'', \quad (16)$$

$$\lambda \Psi - \alpha \xi \Phi = \frac{1}{\kappa} \Psi''. \quad (17)$$

Since  $\Delta' = 2\alpha^2 / \kappa \epsilon \gg 1$ , this eigenvalue problem is mathematically similar to the one solved by Coppi *et al.*<sup>26</sup> for large- $\Delta'$  tearing modes. It reduces to solving the following

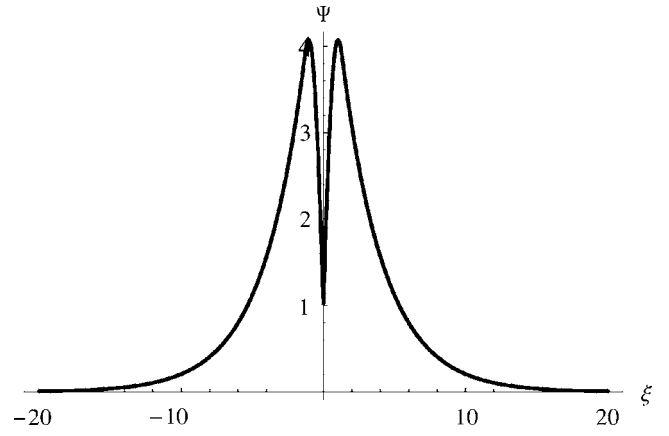


FIG. 3. The outer solution evaluated for  $\epsilon^{-1} = 10^3$  at  $\kappa \approx 340$ , corresponding to the maximum growth rate.

transcendental equation for the growth rate

$$-\frac{\pi}{8} (\kappa \alpha)^{1/3} \Lambda^{5/4} \frac{\Gamma[(\Lambda^{3/2} - 1)/4]}{\Gamma[(\Lambda^{3/2} + 5)/4]} = \Delta' = \frac{2\alpha^2}{\kappa \epsilon}, \quad (18)$$

where  $\Gamma$  is the gamma function and  $\Lambda = \lambda \alpha^{-2/3} \kappa^{1/3}$ . The width of the inner region is given by  $\delta = (\lambda / \kappa)^{1/4} \alpha^{-1/2}$ . Recall that  $\lambda = \gamma / \Gamma_0 \kappa$  and  $\kappa = k_0 v_A / \Gamma_0$ .

Equation (18) has two interesting limits. Assuming  $\Lambda \ll 1$ ,

$$\gamma / \Gamma_0 \approx 1.63 \kappa^{-2/5} \epsilon^{-4/5}, \quad (19)$$

and assuming  $\Lambda \rightarrow 1-$  (from below),

$$\gamma / \Gamma_0 \approx (\alpha \kappa)^{2/3} - \frac{\sqrt{\pi}}{3\alpha} \kappa^2 \epsilon. \quad (20)$$

The maximum growth rate  $\gamma_{\max}$  lies between these two asymptotics. Comparing the two terms in Eq. (20) shows that it is attained for  $\kappa_{\max} \sim \epsilon^{-3/4} \gg 1$  and, therefore,  $\gamma_{\max} / \Gamma_0 \sim \epsilon^{-1/2} \gg 1$ . We note also that  $\kappa_{\max} \epsilon \sim \epsilon^{1/4}$ ,  $\lambda \sim \epsilon^{1/4}$  and the inner layer width  $\delta \sim \epsilon^{1/4}$  for the fastest growing mode. This confirms all of the ordering assumptions we made in our calculation.

Figure 4 shows the dependence  $\gamma(\kappa)$  resulting from the numerical solution of Eq. (18) for two different values of the current sheet aspect ratio  $\epsilon^{-1}$ . Both scalings [Eqs. (19) and (20)] are manifest. The vertical lines identify the values of  $\kappa$  for which  $\kappa \epsilon = 1$ . Strictly speaking, our calculation is only valid for values of  $\kappa$  significantly to the left of this line. This is, however, of secondary importance, as the maximum of the growth rate lies well within the region of validity of our asymptotic ordering for  $\epsilon^{-1} \geq 10^3$ .

We have shown analytically that SP current sheets with large aspect ratios are intrinsically unstable to high-wavenumber perturbations. Since  $\epsilon^{-1} = (S/2)^{1/2}$ , the maximum growth rate scales with the Lundquist number as  $\gamma_{\max} \sim S^{1/4} \Gamma_0$ . Typical Lundquist numbers in plasmas of interest are extremely large (e.g.,  $S \approx 10^{12}$  in the solar corona), so the instability of the current sheet is extremely fast compared to the Alfvén time  $\sim \Gamma_0^{-1}$ . One immediate consequence of this is that stable current sheets with aspect ratios above some critical value cannot exist. Numerical simulations<sup>15,16</sup> suggest

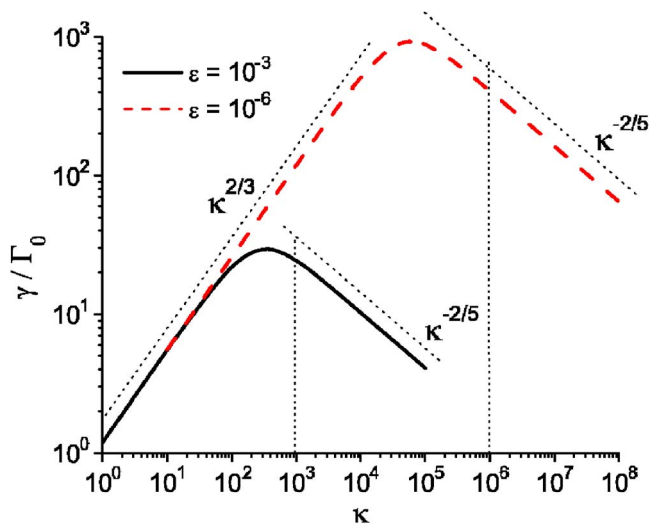


FIG. 4. (Color online) The growth rate calculated from Eq. (18) for two values of the aspect ratio,  $\epsilon^{-1}=10^3$  and  $10^6$ .

that this value is  $\sim 10^2$ , corresponding to  $S_c \sim 10^4$ . Above this value, the sheet breaks up and a chain of plasmoids is formed. Their number scales as  $\kappa_{\max} \sim S^{3/8}$  and their length is  $\sim S^{1/8}$  larger than the current-sheet width  $\delta_{CS}$ .

We note that, as far as we know, no numerical simulations of current sheets with aspect ratios significantly exceeding  $\sim 10^2$  have been reported. At these values, our asymptotic theory is not yet rigorously applicable, so we cannot test it against the existing simulations of SP reconnection. A nonasymptotic extrapolation of our results suggests that only a very small number of plasmoids is to be expected—these are, indeed, seen.<sup>15–18,27,30</sup>

Since the growth rate we have found is much larger than the inverse Alfvén time  $v_A/L_{CS}$ , the plasmoid width should become comparable to the inner-layer width  $\delta \sim S^{-1/8} \delta_{CS}$  before the plasmoids can be expelled from the current sheet by the Alfvénic outflows. The plasmoid evolution then becomes nonlinear. In order to have a quantitative theory of how the plasmoids affect the reconnection, one needs to understand what happens in the nonlinear regime. The dynamics in this regime will be dictated by a competition between three processes: the nonlinear growth and saturation of the plasmoids due to reconnection, the plasmoid coalescence,<sup>28,29</sup> and the expulsion of the plasmoids along the current sheet by the Alfvénic outflows. Numerical results on the stalling of the coalescence instability at large  $S$  suggest that multiple plasmoids can survive in the nonlinear regime rather than coalescing into a single plasmoid.<sup>27</sup> The formation of multiple large plasmoids has also been reported.<sup>18,30</sup> If the width of the plasmoids can indeed become bigger than the width of the current sheet before they coalesce or are expelled, estimates of the SP reconnection time must no longer be based on the parameters of the original current sheet but rather on some effective reconnection region whose width is determined by the saturated plasmoid chain. A nonlinear study of the current sheet instability and plasmoid dynamics, as well as comparing the theory proposed in this Letter against more sophisticated and richer physics models, can only be performed by means of numerical simulations. We are presently

developing a computer code tailored to the study of this problem. Results will be presented in a separate publication.

Discussions with D. A. Uzdensky are gratefully acknowledged. N.F.L. was supported by the Center for Multi-scale Plasma Dynamics, DOE Fusion Science Center Cooperative Agreement ER54785. He thanks the Leverhulme International Network for Magnetised Plasma Turbulence for travel support. A.A.S. was supported by an STFC Advanced Fellowship.

<sup>1</sup>P. A. Sweet, *Annu. Rev. Astron. Astrophys.* **7**, 149 (1969).

<sup>2</sup>J. W. Dungey, *Phys. Rev. Lett.* **6**, 47 (1961).

<sup>3</sup>A. Bhattacharjee, *Annu. Rev. Astron. Astrophys.* **42**, 365 (2004).

<sup>4</sup>T. Yokoyama, K. Akita, T. Morimoto, K. Inoue, and J. Newmark, *Astrophys. J.* **546**, L69 (2001).

<sup>5</sup>C. J. Xiao, X. G. Wang, Z. Y. Pu, H. Zhao, J. X. Wang, Z. W. Ma, S. Y. Fu, M. G. Kivelson, Z. X. Liu, Q. G. Zong, K. H. Glassmeier, A. Balogh, A. Korth, H. Reme, and C. P. Escoubet, *Nat. Phys.* **2**, 478 (2006).

<sup>6</sup>R. J. Hastie, *Astrophys. Space Sci.* **256**, 177 (1997).

<sup>7</sup>E. N. Parker, *J. Geophys. Res.* **62**, 509 (1957).

<sup>8</sup>P. A. Sweet, in *Electromagnetic Phenomena in Cosmical Physics*, edited by B. Lehnert (Cambridge University Press, Cambridge, 1958), p. 123.

<sup>9</sup>H. E. Petschek, in *The Physics of Solar Flares*, edited by W. N. Hess (NASA, Washington, D.C., 1964), pp. 425.

<sup>10</sup>L. M. Malyskhin, T. Linde, and R. M. Kulsrud, *Phys. Plasmas* **12**, 102902 (2005).

<sup>11</sup>J. Birn *et al.*, *J. Geophys. Res.* **106**, 3715, DOI: 10.1029/1999JA900449 (2001).

<sup>12</sup>M. Yamada, H. Ji, S. Hsu, T. Carter, R. Kulsrud, and F. Trinchouk, *Phys. Plasmas* **7**, 1781 (2000).

<sup>13</sup>J. Lin, Y.-K. Ko, L. Sui, J. C. Raymond, G. A. Stenborg, Y. Jiang, S. Zhao, and S. Mancuso, *Astrophys. J.* **622**, 1251 (2005).

<sup>14</sup>Q.-G. Zong *et al.*, *Geophys. Res. Lett.* **31**, 18803, DOI: 10.1029/2004GL020692 (2004).

<sup>15</sup>D. Biskamp, *Phys. Fluids* **29**, 1520 (1986).

<sup>16</sup>N. F. Loureiro, S. C. Cowley, W. D. Dorland, M. G. Haines, and A. A. Schekochihin, *Phys. Rev. Lett.* **23**, 235003 (2005).

<sup>17</sup>W. Daughton, J. Scudder, and H. Karimabadi, *Phys. Plasmas* **13**, 072101 (2006).

<sup>18</sup>J. F. Drake, M. Swisdak, K. M. Schoeffler, B. N. Rogers, and S. Kobayashi, *Geophys. Res. Lett.* **33**, L13105, DOI: 10.1029/2006GL025957 (2006).

<sup>19</sup>K. Shibata and S. Tanuma, *Earth, Planets Space* **53**, 473 (2001).

<sup>20</sup>J. F. Drake, M. Swisdak, H. Che, and M. A. Shay, *Nature (London)* **443**, 553 (2006).

<sup>21</sup>D. A. Uzdensky, *Appl. Spectrosc.* **292**, 573 (2004).

<sup>22</sup>H. P. Furth, J. Killeen, and M. N. Rosenbluth, *Phys. Fluids* **6**, 459 (1963).

<sup>23</sup>S. V. Bulanov, S. I. Syrovatsky, and J. Sakai, *JETP Lett.* **28**, 177 (1978).

<sup>24</sup>D. A. Uzdensky and R. M. Kulsrud, *Phys. Plasmas* **7**, 4018 (2000).

<sup>25</sup>H. R. Strauss, *Phys. Fluids* **19**, 134 (1976).

<sup>26</sup>B. Coppi, R. Galvão, M. N. Rosenbluth, and P. Rutherford, *Sov. J. Plasma Phys.* **2**, 533 (1976).

<sup>27</sup>D. A. Knoll and L. Chacón, *Phys. Plasmas* **13**, 032307 (2006).

<sup>28</sup>J. M. Finn and P. K. Kaw, *Phys. Fluids* **20**, 72 (1977).

<sup>29</sup>D. Biskamp, *Phys. Lett.* **87A**, 357 (1982).

<sup>30</sup>R. Samtaney, S. C. Jardin, P. Colella, and D. F. Martin, in *Adaptive Mesh Refinement—Theory and Applications*, edited by T. Plewa, T. Linde, and V. Gregory (Springer, Berlin, 2005), p. 491.

<sup>31</sup>Going to the next order in our outer solution results in an additional subdominant contribution to  $\Delta'$  comparable to the second term in Eq. (15). Note that while the contribution of the second term in Eq. (13) to  $\Delta'$  is negligible, the term itself cannot be dropped because it ensures that the solution has a finite value at  $\xi=0$ . Note also that there exists an unstable solution that is entirely confined inside the current sheet, so that  $\Psi(\pm\xi_0)=0$ . For this solution,  $C_1^\pm=0$  in Eq. (11) and to the lowest order in  $\kappa^2\epsilon^2$ ,  $\Delta'$  is given just by the second term in Eq. (15). Solving Eq. (10) to the next order in  $\kappa^2\epsilon^2$ , we find  $\Delta'(\kappa)\approx 0.57-1.47\kappa^2\epsilon^2$ . The growth rate then is obtained from Eq. (18) in the limit  $\Lambda\ll 1$ . The result is  $\gamma/\Gamma_0\approx 0.61\kappa^{2/5}\Delta'(\kappa)^{4/5}$ , whence  $\kappa_{\max}\approx 0.28\epsilon^{-1}$  and  $\gamma_{\max}\sim\epsilon^{-2/5}$ . We will not consider this solution because it grows slower than the unconfined mode and its validity hinges on the numerical smallness of  $\kappa_{\max}^2\epsilon^2\approx 0.08$ .